Applied Catalysis A, General 551 (2018) 79–87

Contents lists available at ScienceDirect

Applied Catalysis A, General

journal homepage: www.elsevier.com/locate/apcata

Improving the low-temperature hydrothermal stability of Cu-SAPO-34 by the addition of Ag for ammonia selective catalytic reduction of NO_x

Xiao Xiang[a,b], Yi Cao[a], Lijing Sun[a,b], Pengfei Wu[a,b], Lei Cao[a], Shutao Xu[a], Peng Tian[a,*], Zhongmin Liu[a,*]

[a] National Engineering Laboratory for Methanol to Olefins, Dalian National Laboratory for Clean Energy, Dalian Institute of Chemical Physics, Chinese Academy of Sciences, Dalian, 116023, PR China
[b] University of Chinese Academy of Sciences, Beijing, 100049, PR China

ARTICLE INFO

Keywords:
Cu-SAPO-34
CuAg-SAPO-34
Hydrothermal stability
NH_3-SCR

ABSTRACT

Ag promoted Cu-SAPO-34 has been developed to improve the low-temperature hydrothermal stability of Cu-SAPO-34 for the NH_3-SCR reaction. Kinetic tests show that the addition of Ag into Cu-SAPO-34 doesn't change the reaction mechanism. The ion-exchanged Ag species, which decrease the Brønsted acid density and provide more Lewis acid sites with moderate acidity, have a protective effect on the SAPO framework against low-temperature steaming treatment (LTST). Higher surface Cu content is observed for $CuAg_{2.25}$-SAPO-34, although $CuAg_{2.25}$-SAPO-34 and Cu-SAPO-34 have similar content of isolated Cu ions. *In situ* DRIFTS studies demonstrate, for the first time, the NH_3 molecules adsorbed on the weak/moderate acid sites (independent of the acid types such as Brønsted acid or Lewis acid) are more active than on the strong acid sites for the low-temperature SCR reaction. Compared with the original catalyst Cu-SAPO-34, the enhanced SCR activity of $CuAg_{2.25}$-SAPO-34 after LTST is ascribed to the better preservation of total acid sites, higher moderate acid density (Lewis acid sites) and larger amount of surface Cu species on the $CuAg_{2.25}$-SAPO-34 catalyst.

1. Introduction

The growing applications of diesel engines working under lean-burn conditions generate more nitrogen oxides (NO_x) as the exhaust emissions, which bring about the serious air pollution issue [1]. Over the past two decades, the legislative control has become increasingly stringent so that it requires to find innovative ways for the after-treatment system. Selective catalytic reduction of NO_x with NH_3 (NH_3-SCR) is currently the most promising technique [2], which is generally integrated with diesel particulate filter (DPF) to constitute a diesel emission control system. Therefore, a good hydrothermal stability of the NH_3-SCR catalyst is required to tolerate the periodical regeneration of the DPF (> 650 °C). Traditional NH_3-SCR catalyst V_2O_5/WO_3–TiO_2 for stationary applications is challenging to satisfy the wide temperature range of lean-burn diesel engine. It is mainly due to 1) the possible phase transformation of anatase support [3] and 2) the potential environmental issue with the sublimation of vanadia, which restricts its further application [1,4]. Therefore, metal-exchanged zeolites gain increasing attention in recent decades. However, the early developed catalysts such as Cu-ZSM-5 and Fe-Beta always suffered from the deactivation in the presence of water at high temperatures due to the hydrolysis of acid sites (dealumination), structural degradation and loss of active metal species [5,6]. In addition, the activity of Cu-ZSM-5 (in the high-temperature range) and Fe-Beta (in the low-temperature range) also needs to be improved. More recently, small-pore zeolites and silicoaluminophosphate molecular sieves such as SSZ-13 and SAPO-34 (framework type code: CHA) are recognized to be promising supports for Cu-based NH_3-SCR catalysts with excellent high-temperature hydrothermal stability and superior activity over a wide temperature range. A promising example is the Cu-SAPO-34 catalyst, which can preserve its NH_3-SCR activity at high level even after harsh high-temperature hydrothermal steam treatment [7–9].

Although the high-temperature steam stability of zeolite supports is an important issue for developing NH_3-SCR catalysts, SAPO-34 with silicoaluminophosphate composition is very sensitive to the moisture at room temperature, which is different from the conventional aluminosilicate zeolites [10,11]. The exposure of the calcined SAPO-34 catalyst to humid environment at room temperature for several days may cause severe structural deterioration due to the irreversible hydrolysis of bridge hydroxyl group (Si—OH—Al). And this phenomenon becomes more serious with the increase of Si content in SAPO-34, which can be attributed to the increased bridge hydroxyl group density [12]. Such a

* Corresponding authors.
E-mail addresses: tianpeng@dicp.ac.cn (P. Tian), liuzm@dicp.ac.cn (Z. Liu).

https://doi.org/10.1016/j.apcata.2017.12.001
Received 21 August 2017; Received in revised form 1 December 2017; Accepted 3 December 2017
Available online 05 December 2017
0926-860X/

structural degradation of SAPO-34 also occurs during the process of aqueous ion exchange [13]. The incorporation of Cu^{2+} into SAPO-34 could improve the stabilization of negative Si—O—Al connections and increase its low-temperature hydrothermal stability [14]. However, a structural deterioration is still inevitable after a longer period of exposure to moisture at low temperature (< 100 °C). Moreover, the active Cu species may also decrease and transform into the inactive form [15]. Correspondingly, the catalytic performance of Cu-SAPO-34, especially the low-temperature reactivity, shows an obvious decline [15]. Higher Cu loadings may help preserve the microstructure of SAPO-34 [14], but it would cause the occurrence of a serious side reaction (NH_3 oxidation) at high temperatures [16,17]. Therefore, finding better solutions to improve the low-temperature hydrothermal stability of Cu-SAPO-34 catalyst is essential for its practical application. Pitifully, little progress has been made in this aspect till now.

In the present work, we manage to improve the low-temperature hydrothermal stability of Cu-SAPO-34 by adding a secondary metal species and find that Ag promoted Cu-SAPO-34 behaves a better low-temperature NH_3-SCR activity after low-temperature steaming treatment (LTST) as compared to the original Cu-SAPO-34. Detailed characterizations are employed to investigate the effect of Ag addition on the active Cu species and textural/acidity properties of Cu-SAPO-34. Kinetic tests are also carried out to discriminate the reaction mechanisms between Cu-SAPO-34 and CuAg-SAPO-34. Moreover, *in situ* Diffuse Reflectance Infrared Fourier Transform Spectroscopy (DRIFTS) is employed to clarify the contribution of acid sites with different acid strength (including Brønsted and Lewis acid sites) on the low-temperature NH_3-SCR reaction, which is still ambiguous in the previous studies but important for a better understanding of the reactivity of CuAg-SAPO-34.

2. Experimental

2.1. Catalyst preparation

SAPO-34 was synthesized with a gel composition of 2.0 diethylamine (DEA)/1.0Al_2O_3/1.0P_2O_5/0.8SiO_2/50H_2O. Pseudoboehmite (72.5%), phosphoric acid (85 wt%) and silica sol (30 wt%) were used as Al, P and Si source, respectively. The gel was stirred at room temperature for 30 min and sealed into a stainless steel autoclave, and then crystallized at 200 °C for 24 h under tumbling. After crystallization, the sample was filtered, washed and dried in air.

SAPO-34 with small crystal size (denoted as SAPO-34S) was prepared with a gel composition of 1.5 DEA/1.0 TEACl/1.0Al_2O_3/1.0P_2O_5/0.8SiO_2/40H_2O (200 °C, 24 h). The synthetic procedure was similar to the above-mentioned SAPO-34.

Direct ion exchange method, which was recently reported by us [18], was employed in this work to prepare ion exchanged SAPO-34. The as-synthesized SAPO-34 was directly put into the solution containing target ions without the process of calcination and NH_4^+ exchange and stirred at 50 °C for 4 h. Then the catalysts were centrifuged, washed and dried at 100 °C overnight. To get the final catalyst, a calcination process under air at 600 °C for 5 h was conducted to remove the template.

For the LTST experiment, the calcined samples were treated at 50 °C with 10% H_2O balanced with N_2 (82% relative humidity) for 48 h and then dried at 100 °C overnight. The steam-treated Cu-SAPO-34 and $CuAg_x$-SAPO-34 are named as Cu-SAPO-34/H and $CuAg_x$-SAPO-34/H respectively, where x stands for the Ag content.

For the high-temperature hydrothermal aging, the calcined sample was treated with 8% H_2O and 7.5% O_2 balanced with N_2 at 750 °C for 13 h [9]. The aged samples are named as Cu-SAPO-34/HTA and $CuAg_x$-SAPO-34/HTA respectively.

2.2. Characterizations

Powder X-ray diffraction pattern was conducted on a PANalytical X'Pert PRO X-ray diffractometer with Cu Kα radiation (λ = 1.54059 Å), operating at 40 kV and 30 mA in the range of 5–65° with a step size of 0.026°. SEM was conducted on a Hitachi SU8020. The elemental compositions of the samples were determined by XRF (PANalytical Axios advanced). N_2 adsorption experiments were measured on Micromeritics ASAP2020. The samples were dehydrated at 350 °C for 240 min, and then measured at −196 °C. NH_3-TPD was conducted on Micromeritics Auto Chem II. 0.2 g sample was pretreated at 650 °C for 60 min in He (30 mL/min) and then cooled to 100 °C, 10 mL/min NH_3(6%)/He was then introduced to saturate the sample. After purging the physical absorbed NH_3, a TPD experiment to 650 °C at a rate of 10 °C/min was conducted. The concentration of NH_3 was recorded by a TCD detector.

All the solid state NMR experiments were performed on a Bruker Avance III 600 spectrometer equipped with a 14.1 T wide-bore magnet using a 4 mm MAS probe. The resonance frequencies were 119.2 and 600.13 MHz for ^{29}Si and ^{1}H, respectively. ^{29}Si MAS NMR spectra were recorded with a spinning rate of 8 kHz using high-power proton decoupling. 4096 scans were accumulated with a π/4 pulse width of 2.5 μs and a 10 s recycle delay. Chemical shifts were referenced to 4,4-dimethyl-4-silapentane sulfonate sodium salt (DSS). Before ^{1}H MAS NMR experiment, the samples were dehydrated typically at 420 °C and a pressure below 10^{-3} Pa for 20 h. ^{1}H MAS NMR spectra were recorded with a 4 mm MAS probe. The pulse width was 2.9 μs for a π/2 pulse, and 32 scans were accumulated with a 4 s recycle delay. Samples were spun at 12 kHz, and chemical shifts were referenced to adamantane at 1.74 ppm. All samples were weighed for quantification of Brønsted acid density, and their ^{1}H MAS NMR spectra were resolved by Dmfit software [19] with Gaussian-Lorentz line shapes, using adamantane (1.74 ppm) as the quantitative external standard, measured under the same NMR acquisition condition [20].

XPS was measured on Thermo ESCALAB 250Xi. An Al-kα X-ray source working at 15 kV and 10.8 mA was used and the binding energy was corrected referring C 1s (284.6 eV).

EPR was performed on Bruker A 200. The samples were degassed under heating condition under pressure of 10 μm Hg for 4 h before test, and then sealed into a quartz tube for characterization. During spectral collection, microwave power was 10 mW, and frequency was 9.31 GHz. The sweep width was 2000 G and sweep time was 84 s, modulated at 100 kHz with a 3 G amplitude. A time constant of 41 ms was used. Quantification of isolated Cu^{2+} was conducted by using copper sulfate solution as standard (at −196 °C).

Diffuse reflectance of UV–vis spectra were recorded from 200 to 800 nm on a VARIAN Cary-5000 UV–vis-NIR spectrophotometer equipped with an integration sphere.

In situ DRIFTS experiments were performed on BRUKER TENSOR 27 equipped with a MCT detector and a high temperature chamber with ZnSe windows. The powder was put into an Al_2O_3 crucible with an inner diameter of 5 mm. The DRIFTS spectra were recorded by accumulating 256 scans at a spectral resolution of 4 cm^{-1}. The calcined sample was heated to 600 °C in N_2 (49 mL/min) to purge the absorbed species. Background at each temperature was collected in N_2 separately. For NH_3-TPD experiment, the sample was first saturated with NH_3 at 100 °C and purged with N_2 until the line was stable. Then the sample was heated to each target temperature at a rate of 10 °C/min in N_2 (49 mL/min). The spectra were recorded until the profile was stable. Afterwards, NO + O_2 surface reaction was conducted on the same sample at 150 °C. 930 ppm NO (maybe partially oxidized by O_2 in the mixed feed gas) plus 5% O_2 with N_2 as a balance was passed over the sample pre-saturated with NH_3. The spectra were collected every 5 min until the profile was stable. After NO + O_2 surface reaction, NO was cut off in the feed gas and the sample was purged with 5% O_2 in N_2 until the profile was stable. Then NH_3 (880 ppm) and NO (930 ppm) was added into the 5% O_2/N_2 feed gas which was called NO + O_2 + NH_3

surface reaction(NO maybe partially oxidized by O_2 in the mixed feed gas). The spectra were collected every 5 min until the profile was stable.

2.3. Catalytic activity testing

The standard SCR reaction was conducted at atmospheric pressure in a quartz fixed-bed reactor with an internal diameter of 9.5 mm. 0.1 g calcined catalyst in 60–80 mesh was diluted with 0.4 g quartz (60–80 mesh). The mixture was fixed in the quartz tube with quartz wool. The catalyst was pretreated with N_2 at 600 °C for 40 min and then cooled to the reaction temperature. The feed gas containing 500 ppm NH_3, 500 ppm NO, 5% O_2, 5% H_2O and balance N_2 was then introduced in the reaction system (water vapour was provided by a saturated tube with a liquid-circulating thermostat water bath). The total flow gas for the reaction was 300 mL/min corresponding to a GHSV of 180,000 h^{-1}. FTIR spectrometer (BRUKER TENSOR 27) equipped with a gas cell was used to measure the concentrations of NO, NO_2, N_2O and NH_3. At each reaction temperature, at least 30 min was kept to ensure the achievement of a steady state.

2.4. Kinetics experiments

The kinetics test for standard SCR reaction was conducted in a quartz reactor. 0.01 g catalyst (60–80 mesh) diluted with 0.19 g quartz (60–80 mesh) was used. Volume hourly space velocity of 1,800,000 h^{-1} was used to ensure the elimination of external diffusion. The sample was pretreated at 600 °C for 40 min in N_2 and then cooled to the reaction temperature. The feed gas consists of 500 ppm NO, 500 ppm NH_3, 5% O_2 balanced with N_2. The data was collected in the region where the conversion of NO is under 10%.

3. Results and discussion

3.1. Reaction activity test

CuAg-SAPO-34 and Cu-SAPO-34 catalysts are prepared by direct ion exchange method recently reported by us [18]. This method could simplify the ion exchange procedure and abate the structure degradation of the SAPO framework during ion exchange. The detailed ion exchange conditions and elemental compositions of the samples are listed in Table 1. CuAg-SAPO-34 and Cu-SAPO-34 have good crystallinity and similar Cu content of ~1.4 wt%. The Ag loadings of the three CuAg-SAPO-34 samples are 0.75, 2.25 and 4.83 wt%, respectively.

Fig. 1 presents the NO conversion of the standard NH_3-SCR reaction at low temperature over CuAg-SAPO-34 and Cu-SAPO-34 catalysts before and after low-temperature steaming treatment. The reaction results in the whole temperature range are shown in Fig. S1. All fresh catalysts display similar catalytic activity in the investigated temperature range of 120–550 °C, implying that the addition of Ag to Cu-SAPO-34 has unobvious effect on its apparent NH_3-SCR activity. This is, to some extent, understandable given the inferior low-temperature reaction activity of Ag-SAPO-34, which shows less than 10% NO conversion before 250 °C (Fig. S2). The excellent NH_3-SCR reaction activity over the fresh catalysts, which reaches ~95% of NO conversion at 175 °C and maintains a high level of above 90% until 550 °C, suggests the Cu loading in the catalysts is appropriate. Upon LTST (10% vapour in N_2 at 50 °C for 48 h), all catalysts present a decline of the NO conversion in the temperature range below 250 °C, whereas the activity at higher temperatures is little influenced. It is noted that only a slight decrease of the NO conversion is observed on $CuAg_{2.25}$-SAPO-34 after LTST treatment, evidencing that the addition of Ag to Cu-SAPO-34 could help inhibit the activity decline against the LTST. However, the stability improvement of CuAg-SAPO-34 was not proportional to the Ag content of the catalysts. $CuAg_{4.83}$-SAPO-34/H with the highest Ag content shows an inferior reaction activity than $CuAg_{2.25}$-SAPO-34/H (Fig. 1), indicating that an optimal Ag content exists for the better low temperature hydrothermal stability.

The generation of N_2O is of special concern for SCR catalysts, since N_2O is a greenhouse gas and ozone depletion catalyst. Herein, the concentration of N_2O in the outlet is lower than 10 ppm in the whole reaction temperature range over all the invesitgated CuAg-SAPO-34 and Cu-SAPO-34 catalysts. In addition, the NH_3-SCR reactivity of $CuAg_{2.25}$-SAPO-34 after high-temperature hydrothermal aging is also investigated. The corresponding results are displayed in Fig. S3. It can be seen that after steaming treatment at 750 °C for 13 h, $CuAg_{2.25}$-SAPO-34/HTA possesses a similar reaction behaviour to the fresh $CuAg_{2.25}$-SAPO-34 sample, confirming its excellent high-temperature hydrothermal stability.

Table 1
Ion exchange conditions and elemental compositions of the samples.

Sample[a]	Ion exchange solution (mol/L)		L/S[b]	Metal loading (wt%)[c]	
	$Cu(OAc)_2$	$AgNO_3$		Cu	Ag
Cu-SAPO-34	0.010	–	18	1.40	–
$CuAg_{0.75}$-SAPO-34	0.011	0.003	20	1.45	0.75
$CuAg_{2.25}$-SAPO-34	0.012	0.01	20	1.42	2.25
$CuAg_{4.83}$-SAPO-34	0.015	0.025	20	1.46	4.83

[a] The elemental composition of SAPO-34 precursor is $Al_{0.46}Si_{0.19}P_{0.35}$.
[b] The liquid (mL)/solid (g) ratio for ion exchange (50 °C, 4 h).
[c] The metal content is determined by XRF.

3.2. Kinetic experiment

The addition of another type of transitional metal into Cu-SAPO-34 may cause an alteration of the reaction route. Kinetic experiment was conducted to investigate the mechanism of the standard NH_3-SCR reaction on $CuAg_{2.25}$-SAPO-34 and Cu-SAPO-34. A similar apparent activation energy of around 30 kJ/mol is observed on both Cu-SAPO-34 and $CuAg_{2.25}$-SAPO-34 catalysts (Fig. 2a). This value is lower than the previously reported data [21]. Given that NH_3-SCR reaction on CHA-type zeolites is internal diffusion-controlled [21], the apparent activation energy measured maybe modified by internal diffusion limitation and cannot reflect the intrinsic nature of the reaction [13]. To attenuate the influence of the internal diffusion limitation, SAPO-34S with small crystal size of 300 nm was synthesized (XRD and SEM results shown in Figs. S4 and S5, respectively). Cu-SAPO-34S and CuAg-SAPO-34S were prepared following the same protocol as Cu-SAPO-34 and $CuAg_{2.25}$-SAPO-34, respectively. As shown in Fig. 2a, it is calculated that the apparent activation energies are *ca.* 66–67 kJ/mol for both samples, which are much higher than the value observed on the larger crystal catalysts, close to the values of Gao et al. [21]. This provides a strong evidence for the existence of intracrystal diffusion limitation in Cu-SAPO-34 and $CuAg_{2.25}$-SAPO-34. The similar values of activation energies over Cu-SAPO-34S and CuAg-SAPO-34S also suggest that they share the same reaction mechanism.

We further conducted the kinetic experiments in a wider temperature range on Cu-SAPO-34S and Cu-SAPO-34. Fig. 2b shows that the apparent reaction activation energy of Cu-SAPO-34S decreases with the increasing temperature, which should correspond to the transition from dynamic controlled region to diffusion controlled region. However, there is not such a trend for Cu-SAPO-34 with a large crystal of 7–8 μm (a uniform slope), implying the internal diffusion limitation in the tested temperature range. Thus, it is inferred that the apparent reaction activation energy of standard NH_3-SCR reaction on small crystalline catalysts at low temperature range is close to the intrinsic activation energy.

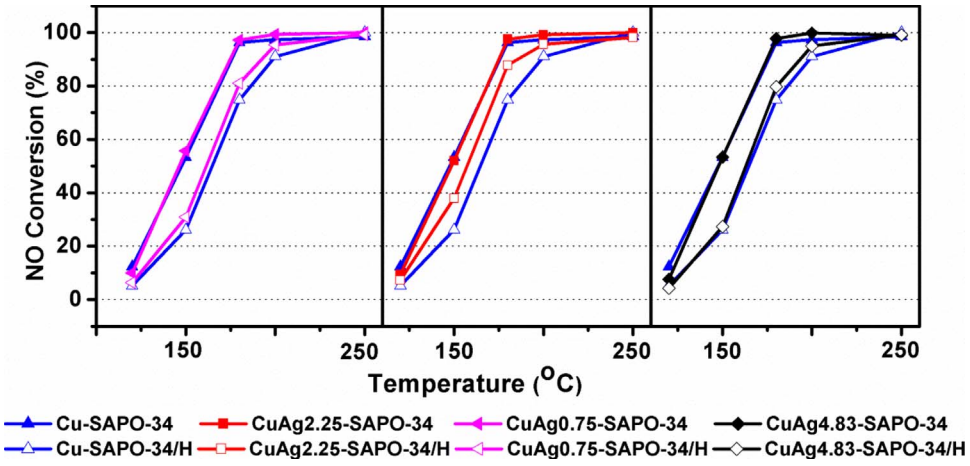

Fig. 1. Standard NH_3-SCR results on CuAg-SAPO-34 and Cu-SAPO-34 at low temperature before and after low-temperature steaming treatment. The feed gas consists of 500 ppm NO, 500 ppm NH_3, 5% O_2 and 5% H_2O balanced with N_2. GHSV = 180,000 h^{-1}.

3.3. Catalyst microstructure determined by N_2 physisorption and solid-state MAS NMR

The textural properties of $CuAg_{2.25}$-SAPO-34 and Cu-SAPO-34 catalysts before and after LTST are investigated by N_2 physisorption. As shown in Table 2, a dropping trend of the BET surface area could be observed with the increase of the ion-exchange level. It implies that ion-exchange treatment could still partially damage the framework of SAPO molecular sieves [13], even though the direct ion-exchange method employed here could protect the structure to a great extent [18]. This should be mainly caused by the weak acidity of the ion-exchange solution. After LTST, both Cu-SAPO-34/H and $CuAg_{2.25}$-SAPO-34/H show a little decrease of the BET surface area as compared with their precursors, suggesting that they keep good structural integrity under the present LTST conditions. However, this is somewhat unexpected considering their deactivation at the low-temperature range in the deNO_x reaction, especially for the Cu-SAPO-34 sample.

^{29}Si MAS NMR is further employed to detect the change of local atomic environments of the catalysts before and after LTST. As shown in Fig. 3, the ^{29}Si NMR spectra give overlapped resonances at −90.6, −95.0, −99.8, −105.2, −110.4 and −115.3 ppm, which could be attributed to $Si(OAl)_2(OSi)_1(OH)$ (Si species in defect sites) [22,23], Si (4Al), Si(3Al), Si(2Al), Si(1Al) and Si(0Al) species, respectively [24,25]. The high-field shifts of the resonance signals following the decrease of Al number coordinated to the Si atom are due to the enhancement of the shielding effect of electrons. The structure of the defect sites is shown in Scheme . The appearance of multiple Si species in the samples is in accordance with the high Si content of the SAPO-34 matrix. The corresponding deconvoluted results of different Si species are given in Table 3. Clearly, the fresh $CuAg_{2.25}$-SAPO-34 and Cu-SAPO-34 catalysts possess similar Si distribution with Si(4Al) environment as the dominate species. After LTST, an obvious increased proportion of the Si species in defect sites could be observed at the expense of Si(4Al) species for both Cu-SAPO-34/H and $CuAg_{2.25}$-SAPO-34/H, indicating the partial degradation of the SAPO framework. More specifically, the Si(4Al) content of Cu-SAPO-34 drops from 45% to 19% (a 26% decrease) and the amount of defect sites rises from 5% to 27% (a 22% increase), whereas a 13% decrease of Si(4Al) content and 12% increase of Si defect sites are observed on $CuAg_{2.25}$-SAPO-34. This implies that Cu-SAPO-34 undergoes more serious structure degradation than $CuAg_{2.25}$-SAPO-34, suggesting the protective effect of Ag addition on the framework of SAPO-34 against the LTST (shown in Scheme). That is, the addition of Ag into Cu-SAPO-34 improves the low-temperature hydrothermal stability of the SAPO framework by partially inhibiting the hydrolysis of acidic Si—OH—Al.

Table 2
Textual properties of the catalysts before and after low temperature steaming treatment.

Sample	Surface area (m^2/g)		Pore volume (cm^3/g)	
	S_{BET}	S_{micro}	V_{micro}	V_{total}
Cu-SAPO-34	482.90	471.15	0.23	0.26
Cu-SAPO-34/H	469.17	459.76	0.22	0.26
$CuAg_{2.25}$-SAPO-34	461.72	453.41	0.22	0.25
$CuAg_{2.25}$-SAPO-34/H	448.38	440.66	0.22	0.25
SAPO-34	525.01	515.08	0.25	0.29

The ^{29}Si NMR results of the samples also suggest that N_2 physisorption is not very sensitive to the structural change of molecular

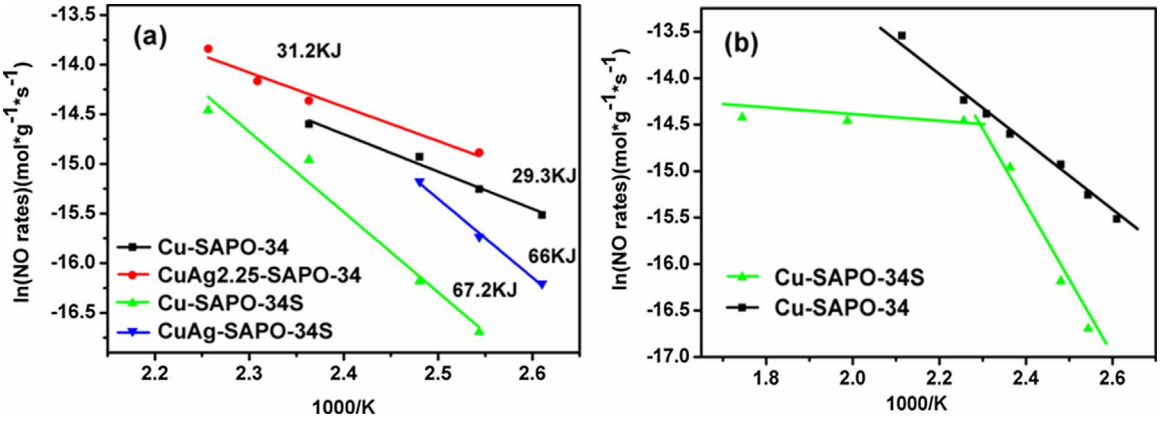

Fig. 2. The kinetic results of NH_3-SCR over the catalysts: (a) Cu-SAPO-34 and CuAg-SAPO-34 with two different crystal sizes; (b) Cu-SAPO-34 with two different crystal sizes in a wide temperature range.

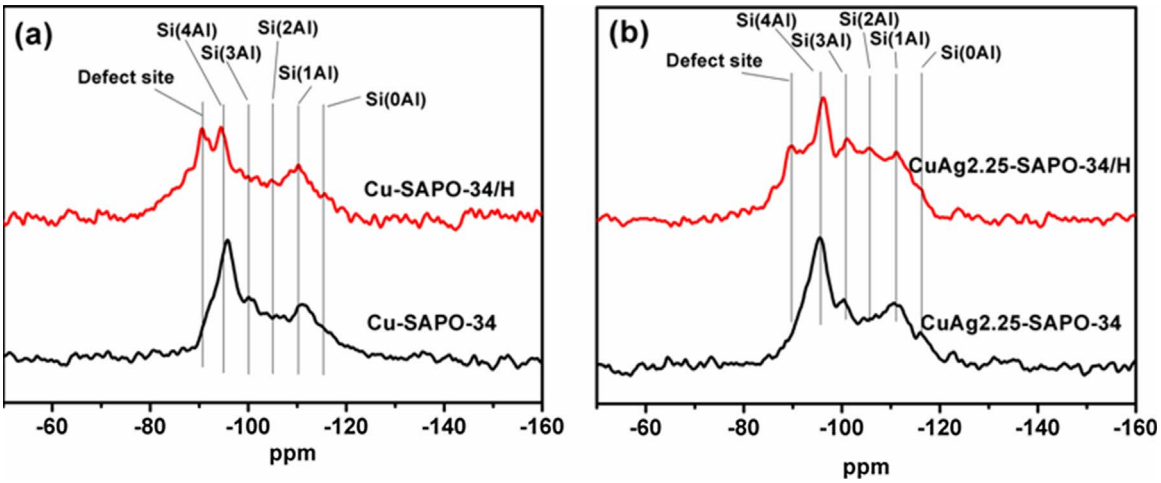

Fig. 3. ^{29}Si MAS NMR spectra of Cu-SAPO-34 and $CuAg_{2.25}$-SAPO-34 before and after LTST.

sieves. Solid state NMR is more helpful to provide easy access to the fine structural information and describe the local microstructure of the solids.

^{1}H MAS NMR is measured to determine the Brønsted acid sites originating from the protons on the bridge hydroxyls. The results are shown in Table 4. The fresh Cu-SAPO-34 has higher Brønsted acid density than $CuAg_{2.25}$-SAPO-34 due to the occupation of Brønsted acid sites by Ag^{+} ions. Upon LTST, the Brønsted acid sites of Cu-SAPO-34 show a drop of 0.18 mmol/g. However, a smaller decrease of 0.11 mmol/g is detected for $CuAg_{2.25}$-SAPO-34, confirming the suppression of the hydrolysis of bridged hydroxyls (Brønsted acid sites) by the addition of Ag.

3.4. XPS and EPR results

XPS measurements are used to investigate the chemical state of Cu and Ag in the $CuAg_{2.25}$-SAPO-34 and Cu-SAPO-34 catalysts (Figs. S6 and S7). Cu-SAPO-34, $CuAg_{2.25}$-SAPO-34/H and Cu-SAPO-34 display similar XPS profiles with almost identical peak positions. The peaks at 933.1 and 952.7 ev could be attributed to Cu $2p_{3/2}$ and Cu $2p_{1/2}$, respectively [26,27]. It is supposed that the incorporated Ag has no (or very less) interactions with the Cu species in the sample and thus does not alter the chemical state of Cu. Otherwise, a shift of the peak position would be expected. Fig. S7 shows the Ag 3d XPS spectra of $CuAg_{2.25}$-SAPO-34 and $CuAg_{2.25}$-SAPO-34/H, in which the peaks located at low and high BE can be attributed to Ag $3d_{5/2}$ and Ag $3d_{3/2}$, respectively. Each peak could be further deconvoluted into two peaks. The peaks at around 368 and 374 ev are responsible for Ag^{+}, while those at around 370 and 376 ev evidence the existence of Ag^{0} [28]. Clearly, most Ag species exist in the form of Ag^{+} ions. The trace amount

Table 3
The deconvoluted results of different Si species based on the ^{29}Si MAS NMR spectra of the samples.

Sample	Defect site	Si(4Al)	Si(3Al)	Si(2Al)	Si(1Al)	Si(0Al)
Cu-SAPO-34	0.05	0.45	0.12	0.12	0.21	0.05
Cu-SAPO-34/H	0.27	0.19	0.16	0.13	0.21	0.04
$CuAg_{2.25}$-SAPO-34	0.05	0.43	0.13	0.15	0.21	0.04
$CuAg_{2.25}$-SAPO-34/H	0.17	0.30	0.12	0.18	0.20	0.03

Table 4
Brønsted acid density of the catalysts before and after low temperature steaming treatment.

Sample	Before (B) (mmol/g)[a]	After (A) (mmol/g)[a]	B-A (mmol/g)
Cu-SAPO-34	1.19	1.01	0.18
$CuAg_{2.25}$-SAPO-34	0.86	0.75	0.11

[a] Determined by ^{1}H MAS NMR.

Table 5
Surface atom ratio of the samples from XPS and XRF.

	Cu-SAPO-34	$CuAg_{2.25}$-SAPO-34		$CuAg_{2.25}$-SAPO-34/H	
	Cu/Al	Ag/Al	Cu/Al	Ag/Al	Cu/Al
XPS	0.020	0.072	0.027	0.075	0.026
XRF	0.029	0.028	0.030	0.028	0.030

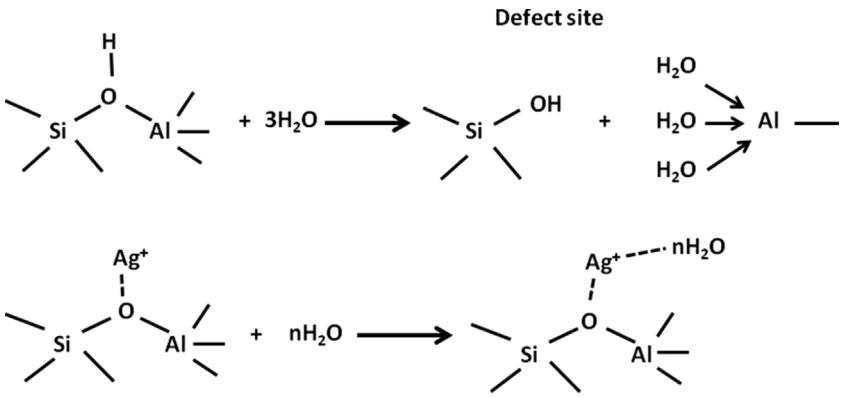

Scheme 1. Hydrolysis of bridge hydroxyl and protection effect of Ag^{+} on the framework.

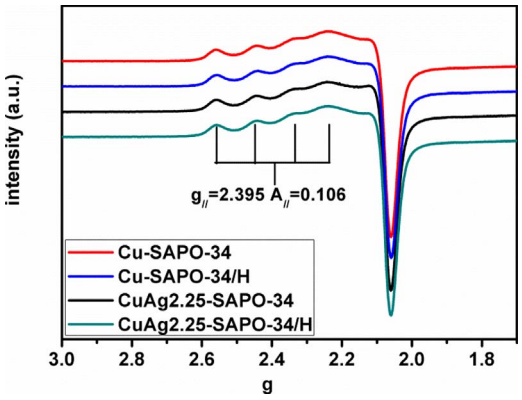

Fig. 4. The EPR spectra of the samples before and after low temperature steaming treatment.

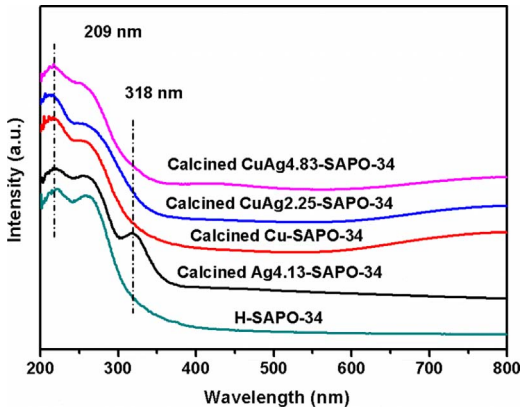

Fig. 5. The UV–vis spectra of the calcined catalysts. The spectra were collected with $BaSO_4$ as background.

of Ag^0 might come from the unexpected reduction of Ag^+ by X-ray beam during the spectra collection. The quantitative results of surface Cu/Al and Ag/Al atom ratio are shown in Table 5. $CuAg_{2.25}$-SAPO-34 possesses a higher surface Cu/Al ratio than Cu-SAPO-34, though both samples have similar bulk Cu/Al ratio as measured by XRF. This means that the concentration of Cu species on the external surface of $CuAg_{2.25}$-SAPO-34 crystals is higher than that of Cu-SAPO-34. Since the NH_3-SCR reaction on SAPO-34 is restricted by internal diffusion limitation [13], the higher surface Cu content on $CuAg_{2.25}$-SAPO-34 herein is expected to benefit the reaction. It would offset, at least partially, the negative effect by the decrease of Brønsted acid density due to the incorporation of Ag, which consequently contributes to the similar reaction activity of the two fresh samples. On the other hand, it should be noted that an obvious surface Ag enrichment phenomenon exists for CuAg-SAPO-34, which possibly results from the larger radius of hydrated Ag ion causing its diffusional limitation into the core of the crystals.

EPR is responsive to isolated Cu^{2+} but silent for other copper species [7]. It is an effective method to study the chemical state and location of Cu^{2+} both qualitatively and quantitatively. Fig. 4 shows the EPR spectra of Cu-SAPO-34 and $CuAg_{2.25}$-SAPO-34. All four samples display similar profiles, in which only one type of Cu species with signals of $g_{//} = 2.395$ and $A_{//} = 0.106$ can be determined. It implies that the isolated Cu^{2+} ions in the samples are in similar chemical environments, which dominantly locates in site (I) of the CHA cage [29–31]. Basically, the Cu^{2+} ions in site (I) for the Cu-SAPO-34 samples have an axial symmetry and octahedrally coordinate to three framework oxygen atoms and three water molecules [29]. These results suggest that both Ag addition and low-temperature steaming treatment have little effect on the location of Cu^{2+} in the catalysts. The quantitative results from EPR for the samples are shown in Table 6. The population of Cu^{2+} species is almost unchanged after the LTST, indicating that the ion-exchanged Cu^{2+} species is quite stable during the exposure to low temperature moisture. Our previous study has revealed that there exists an optimal Cu content for high-silica Cu-SAPO-34 to help more isolated Cu^{2+} survive LTST (Table S1). An extremely high or low ion-exchange level of Cu-SAPO-34 catalysts would lead to a loss of the isolated Cu^{2+} upon LTST, the Cu^{2+} in Cu-SAPO-34 with a moderate ion-exchange level like in this work is relatively stable.

The XPS and EPR results demonstrate that the addition of Ag does not change the chemical state and the location of Cu^{2+} in the samples. Also, there is no interaction between Cu and Ag in the $CuAg_{2.25}$-SAPO-34 catalyst. These results imply that Cu and Ag may work separately and play different roles in the NH_3-SCR reaction.

Table 6
Isolated Cu^{2+} from EPR on the samples before and after low temperature steaming treatment.

Sample	Before (wt%)	After (wt%)	After/Before[a]
Cu-SAPO-34	1.216%	1.240%	1.02
$CuAg_{2.25}$-SAPO-34	1.155%	1.131%	0.98

[a] The ratio of Cu^{2+} content in the samples after and before LTST.

3.5. UV–vis spectra

UV–vis is also employed to investigate the chemical state of Cu and Ag species. From Fig. 5, obvious adsorption bands around 209 and 600–800 nm could be observed for catalysts containing Cu as compared to H-SAPO-34. They are attributed to the LMCT (ligand to metal charge transfer) from oxygen to Cu^{2+} and the d-d transition of Cu^{2+} [32,33], respectively. The spectrum of $Ag_{4.13}$-SAPO-34 displays a clear absorption at 318 nm arising from metallic Ag clusters, suggesting the aggregation of Ag atoms [34]. Because the signals of isolated Ag^+ is generally weak and appears around 215 nm (due to $4d^{10}$-$4d^9 5s^1$ transitions in Ag^+) [28], it is thus difficult to identify the existence of Ag^+ using UV–vis. Interestingly, nearly no absorption due to metallic Ag clusters could be observed for CuAg-SAPO-34 samples (except for very weak band around 318 nm for $CuAg_{4.83}$-SAPO-34), which suggests that the better dispersity of Ag in CuAg-SAPO-34 than in Ag-SAPO-34. That is, the existence of Cu promotes the dispersity of Ag atoms.

3.6. Acidity of the catalysts

NH_3-TPD experiments are conducted to study the acid properties of the catalysts. The profiles and the corresponding deconvoluted results are shown in Fig. 6 and Table S2, respectively. The NH_3-TPD profiles of all samples could be deconvoluted into three peaks centered around

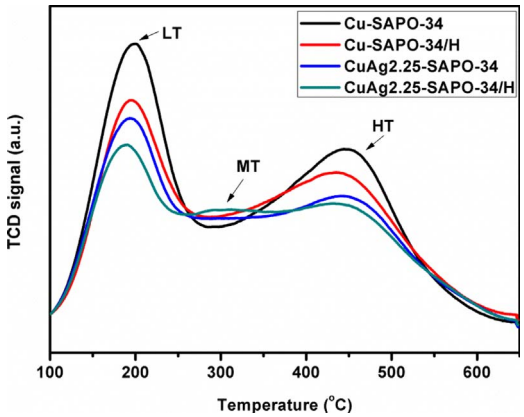

Fig. 6. The NH_3-TPD curves of Cu-SAPO-34 and $CuAg_{2.25}$-SAPO-34 before and after low temperature steaming treatment.

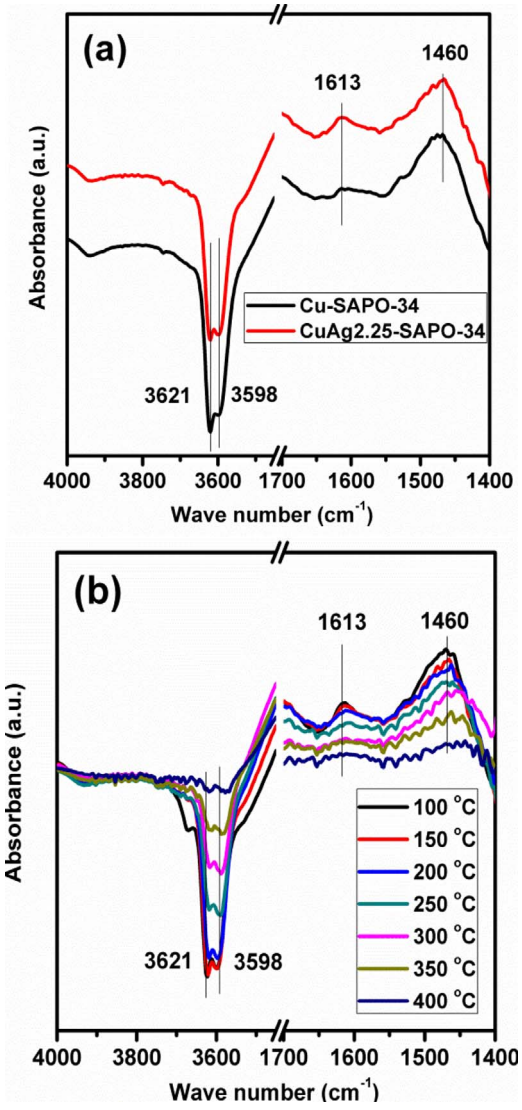

Fig. 7. (a) DRIFTS spectra of NH_3 adsorbed on $CuAg_{2.25}$-SAPO-34 and Cu-SAPO-34 at 150 °C; (b) *In situ* DRIFTS spectra of NH_3-TPD on $CuAg_{2.25}$-SAPO-34 at different temperatures. The spectrum at each temperature is a stable result by purging with N_2. All the spectra in this figure are difference spectrum.

190, 300 and 440 °C. The low-temperature (LT) desorption peak, corresponding to weakly bound

NH_3, may contain the contributions of physisorbed NH_3, NH_3 molecules solvating the NH_4^+ ions (*e.g.* in $N_2H_7^+$ dimers) [35–37], NH_3 adsorbed on terminal P(OH) [38] or Al(OH) with weak acidity. Therefore, a clear assignment of the LT peak is difficult and it is only partially related to the weak acid sites of the catalysts. The medium-temperature (MT) and high-temperature (HT) peaks correspond to acid sites with moderate and strong acid strength, respectively. Given the fact that the fresh $CuAg_{2.25}$SAPO-34 sample shows an increased MT peak at the expense of the LT and HT peaks as compared to Cu-SAPO-34, it is speculated that the incorporated Ag^+ ions occupy part of Brønsted acid sites, provide additional Lewis acid sites and contribute to the increase of MT peak. This is similar to the effect of Cu^{2+} incorporation [39]. On the other hand, because the Brønsted acid sites in sample $CuAg_{2.25}$SAPO-34 may cover a wide range of acid strength from weak to strong acidity due to the existence of different chemical environments (see the following part and Fig. 7), herein the MT peak is attributed to the NH_3 desorbed from both Brønsted and Lewis acid sites. The HT peak is mainly ascribed to the NH_3 desorbed from ammonium ions (NH_4^+) formed over the strong Brønsted acid sites (the bridge hydroxyl groups Si(OH)Al) [40,41].

Both samples suffer a decline of the LT and HT peaks in the NH_3-TPD profiles upon LTST, suggesting the decrease of weakly bound NH_3 (partially associated with weak acid sites) and strongly bound NH_3 (strong acid sites). The decreasing degree of the LT and HT peaks in Cu-SAPO-34 is bigger than in $CuAg_{2.25}$-SAPO-34 (Table S2), consistent with the more serious structure degradation of the former sample as revealed by ^{29}Si NMR. Meanwhile, the moderate acid density of both steam-treated samples increase, due to the generation of Lewis acid sites with medium acidity from the hydrolysis of Si(OH)Al. Notablely, $CuAg_{2.25}$-SAPO-34/H still possesses larger amount of moderate acid sites. To gain further insight in the nature of the acid sites in the catalysts, IR spectra of NH_3 adsorption are collected. Fig. 7a shows the DRIFTS difference spectra of fresh catalysts $CuAg_{2.25}$-SAPO-34 and Cu-SAPO-34 after NH_3 adsorption followed by purging with N_2 at 150 °C. The peak at 1613 cm^{-1} could be attributed to the absorbed NH_3 on Lewis acid sites (bending vibrations of the N—H bonds in the NH_3 molecules) [38,42–44]. The peak at 1460 cm^{-1} arises from bending vibrations of NH_4^+ species resulted from NH_3 protonation over acidic hydroxyl sites [38,44]. In the region of OH stretching vibrations, negative peaks at 3598 and 3621 cm^{-1} are detected, which are due to the depletion of Si—OH—Al groups by NH_3 adsorption [38,45,46]. It is known that there are one T atom site and four different O sites in the CHA framework. These two peaks should correspond to the acidic OH groups sitting in different oxygen environments [23,38,47]. However, an explicit assignment is difficult because the acid strength sequence associated with the four O sites is still under debate. In Fig. 7a, $CuAg_{2.25}$-SAPO-34 shows a relatively stronger absorption band at 1613 cm^{-1} and a higher ratio of Lewis / Brønsted acid sites than Cu-SAPO-34, which should result from the incorporation of Ag and is consistent with the above NH_3-TPD results.

Furthermore, DRIFTS spectra of NH_3 desorption at different temperatures over $CuAg_{2.25}$-SAPO-34 are also recorded and displayed in Fig. 7b. Below 150 °C, the peak intensities of 3598/3621 and 1613 cm^{-1} show no obvious change, while a small decrease at 1460 cm^{-1} could be observed possibly due to the removal of NH_3 adsorbed on the terminal P(OH) and Al(OH) with weak Brønsted acidity. Afterwards, the NH_3 absorbed on Lewis acid sites (1613 cm^{-1}) desorbs with the increasing temperature and nearly completely desorbs at 300 °C. However, there is still a certain amount of NH_3 adsorbed on Brønsted acid sites at this temperature. It implies that the Lewis acid sites in the catalysts have moderate acidity, whereas the Brønsted acid sites cover a wide range of acid strength from weak to strong acidity. Meanwhile, the OH bridging bands (3598 and 3621 cm^{-1}) present a gradual recovery after 200 °C following the desorption of NH_3.

3.7. Relationship between NH_3 adsorption and reactivity at low temperature

In situ DRIFTS experiments under NH_3-SCR reaction conditions are performed to reveal/discriminate the contribution of acid sites with different acid strength to the low-temperature NH_3-SCR activity. This is important for a better understanding of the reaction behaviour of $CuAg_{2.25}$-SAPO-34 and Cu-SAPO-34. Firstly, feed gas containing 930 ppm NO and 5% O_2 in N_2 was passed over the NH_3 pre-adsorbed $CuAg_{2.25}$-SAPO-34 at 150 °C. As shown in Fig. 8a, the intensity of the band at 1613 cm^{-1} is almost consumed after exposure to NO + O_2 for 20 min, implying that the NH_3 adsorbed on Lewis acid sites is highly reactive at low temperature in the presence of NO and O_2. Little change could be observed for the band at 1460 cm^{-1} at this moment. Meanwhile, the intensities of the bands at 3598 and 3621 cm^{-1} decrease by around 50% after the 20 min exposure, evidencing the removal of NH_3 and the recovery of OH bridging sites. The mismatch of the intensity change between the bands at 1460 and 3598/3621 cm^{-1} suggests the contribution of other NH_4^+ ions to the band at 1460 cm^{-1} besides the NH_4^+ associated with Brønsted acid sites. Wang et al. recently reported similar phenomenon on Cu-SAPO-34 and attributed this to the

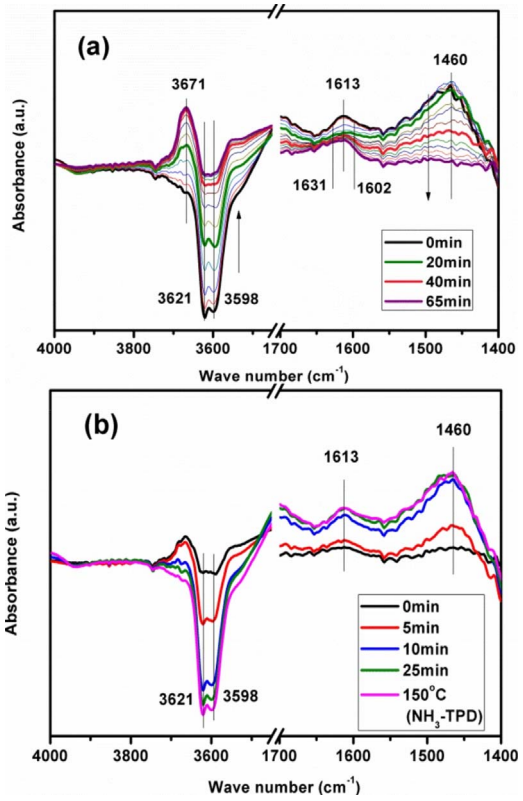

Fig. 8. *In situ* DRIFTS spectra at 150 °C: (a) NO + O_2 surface reaction with pre-absorbed NH_3 on $CuAg_{2.25}$-SAPO-34. The feed gas contains 930 ppm NO and 5% O_2 in N_2. The arrows show the time sequence. Time interval is 5 min; (b) NO + O_2 + NH_3 surface reaction on $CuAg_{2.25}$-SAPO-34. The feed gas contains 930 ppm NO, 880 ppm NH_3 and 5% O_2 in N_2. NH_3-TPD profile at 150 °C in Fig. 7b is displayed here as a comparison. All the spectra in this figure are difference spectrum.

contribution of the formed NH_4NO_x on Lewis acid sites (Cu sites) [38]. Therefore, it is more reasonable to analyse the reactivity of NH_3 on Brønsted acid sites in the NH_3-SCR reaction based on the bands at 3598/3621 cm^{-1}. From Fig. 8a, it is estimated that the NH_3 species adsorbed on Brønsted acid sites (3598/3621 cm^{-1}) run out after 40 min. The band at 1460 cm^{-1} could be clearly observed at this time, which completely disappears after 65 min due to the slow decomposition rate of NH_4NO_x on the catalyst surface at 150 °C. It is interesting to note that the IR intensity of the bands at 3598/3621 and 1613 cm^{-1} after reaction for 10 and 15 min have a close similarity to those of the NH_3-TPD curves at 200 and 250 °C, respectively (Fig. S8), suggesting that the consumption sequence of NH_3 on Lewis and Brønsted acid sites is in accordance with the acid strength of both acid sites. In other words, the firmly bounded NH_3 is not as active as the NH_3 adsorbed on the weak/moderate acid sites for the low-temperature NH_3-SCR reaction.

New bands at 1602, 1613 and 1631 cm^{-1} could be detected after 20 min exposure, the wave number of which are close to the IR band of NH_3 adsorbed on the Lewis acid sites. Given that these bands become stronger with time and the firmly bounded NH_3 on Brønsted acid sites show a gradual decrease, it is unreasonable to assign these bands to the NH_3 on Lewis acid sites. Meanwhile, a band at 3671 cm^{-1} is observed with the appearance of the bands at 1602, 1613 and 1631 cm^{-1}. The position of this peak is rather close to that of P—OH band [8,16,38]. In order to clarify the origin of these bands, 930 ppm NO and 5% O_2 in N_2 was passed over NH_3 pre-saturated Cu-SSZ-13 and H-SAPO-34 at 150 °C (Fig. S9). Similar phenomena on the $CuAg_{2.25}$-SAPO-34 catalyst could be observed over both samples. Since Cu-SSZ-13 does not contain P species, the signal at 3671 cm^{-1} is not supposed to come from P-OH. The appearance of these peaks on H-SAPO-34 also excludes their relation with Cu species. If we further cut off NO in the NO/O_2 gas feed and purge $CuAg_{2.25}$-SAPO-34 with 5% O_2 balanced with N_2 (Fig. S10), an obvious decrease of these peaks could be observed, suggesting that the peaks should arise from the weakly adsorbed species associated with NO or NO_2 [38,48,49].

The reaction performance of NO + O_2 with NH_3 adsorbed over Cu-SAPO-34 at 150 °C is also investigated and the results are shown in Fig. S11. Similar phenomena to those over $CuAg_{2.25}$-SAPO-34 have been observed, confirming the higher reactivity of NH_3 adsorbed on weak/moderate acid sites for the low-temperature SCR reaction.

NO + O_2 + NH_3 surface reaction is conducted over $CuAg_{2.25}$-SAPO-34 at 150 °C (Fig. 8b). It can be seen that both the Lewis acid sites (1613 cm^{-1}) and Brønsted acid sites (3598/3621 cm^{-1}) of the catalyst are gradually covered by NH_3 following the interaction with NO + O_2 + NH_3. And the collected stable spectrum is rather similar to that of NH_3 absorption at 150 °C in the above DRIFTS of NH_3-TPD. It is thus inferred that NH_3 species which could desorb below 150 °C are more active for the SCR reaction at this temperature. It means that the availability/reactivity of NH_3 on the weak and moderate acid sites is better than that on the strong acid sites for the low-temperature SCR reaction, whatever be the acid type (Brønsted or Lewis acid sites). Only when the NH_3 supply on weak/moderate acid sites is insufficient, the strongly adsorbed NH_3 might take part in the reaction, as shown by the results of NO + O_2 surface reaction in Fig. 8a.

3.8. Understanding the low-temperature NH_3-SCR activity over the catalysts before and after LTST

Generally, for Cu-based zeolitic catalysts, both the acidity and Cu species are regarded as two crucial roles for the NH_3-SCR activity. Since the above results have shown that Ag-SAPO-34 has inferior SCR reaction activity and the Ag addition into Cu-SAPO-34 does not change the reaction mechanism and the chemical state of Cu species (Ag species have little interaction with the Cu species in the $CuAg_{2.25}$-SAPO-34 catalyst), we will try to analyse the variation of the reaction activity from the viewpoints of the acidity and active Cu species.

For the fresh Cu-SAPO-34 and $CuAg_{2.25}$-SAPO-34, both catalysts have similar amount of Cu loadings and active Cu^{2+} species; however, the latter sample possesses higher surface Cu content as revealed by XPS, which would benefit the SCR reaction due to the easy accessibility. In addition, although the fresh $CuAg_{2.25}$-SAPO-34 shows reduced LT and HT peaks in the NH_3-TPD curves as compared with Cu-SAPO-34, it possesses higher MT peak due to the contribution of the loaded Ag ions (having Lewis acid sites with moderate acidity). The higher Lewis acid density in $CuAg_{2.25}$-SAPO-34 is also confirmed by DRIFTS spectra. According to our findings in the above section, the NH_3 molecules adsorbed on the Brønsted and Lewis acid sites with weak/moderate acidities are more active for the low-temperature NH_3-SCR reaction. Herein, the higher concentration of surface Cu species and larger amount of Lewis acid sites over $CuAg_{2.25}$-SAPO-34 are believed to help the sample to behave similar NH_3-SCR reaction performance to Cu-SAPO-34.

Upon LTST, the two catalysts preserve their active Cu^{2+} species well, but suffer different structure deterioration, which causes a decreased LT/HT peaks and increased MT peak (due to the formation of defect Al species) as shown in the NH_3-TPD profiles. Although the LT peak in the NH_3-TPD profiles is partially associated with the weak acid sites, this decrease causes a decline in the low-temperature NH_3-SCR reaction activity for both Cu-SAPO-34/H and $CuAg_{2.25}$-SAPO-34/H. On the other hand, since $CuAg_{2.25}$-SAPO-34/H maintains better local microstructure than Cu-SAPO-34/H due to the protection of Ag to the framework, a smaller drop of low-temperature NH_3 desorption amount in the NH_3-TPD curves is observed for $CuAg_{2.25}$-SAPO-34/H. Meanwhile, $CuAg_{2.25}$-SAPO-34/H possesses a larger amount of moderate acid density and higher surface Cu content. These positive factors work together to facilitate $CuAg_{2.25}$-SAPO-34/H to behave better low-

temperature NH_3-SCR reaction activity than Cu-SAPO-34/H.

Characterizations of $CuAg_{4.83}$-SAPO-34 with high Ag loading were also carried out and displayed in Supporting Information (Fig. S12 and Table S2, S3). It demonstrates that upon LTST the isolated Cu ions content shows a small drop and both the moderate and total acid sites decrease, which are relatively serious as compared to those of $CuAg_{2.25}$-SAPO-34 and are believed to result in its lower NH_3-SCR reactivity than $CuAg_{2.25}$-SAPO-34/H. Moreover, we have investigated the influence of the addition of other dopants such as Zn and Ce. As shown in Fig. S13, they all present improved stability against LTST as compared to Cu-SAPO-34, although Ag promoted Cu-SAPO-34 behaves the best catalytic performance. It is mentioned that the small pore size of SAPO-34 might limit the incorporation of some metal ions [18]. Only the ions incorporated into SAPO-34 can have the possibility to enhance the stability of Cu-SAPO-34 against LTST.

4. Conclusions

CuAg-SAPO-34 catalyst has been successfully developed to improve the tolerance of Cu-SAPO-34 to the low-temperature moisture, which is an important issue for the practical application of Cu-based SAPO NH_3-SCR catalyst. $CuAg_{2.25}$-SAPO-34 shows the best low-temperature hydrothermal stability and is also rather stable when exposed to high-temperature hydrothermal aging. Kinetic tests and multiple characterization techniques are applied to explore the better preserved NH_3-SCR activity of $CuAg_{2.25}$-SAPO-34 catalyst against the LTST. It is revealed that NH_3-SCR reaction over the Cu-based SAPO catalysts is internal diffusion-controlled; $CuAg_{2.25}$-SAPO-34 and Cu-SAPO-34 share the same reaction mechanism, and no interactions between Ag and Cu species exist on the $CuAg_{2.25}$-SAPO-34. The addition of Ag ions, which offers a protective effect on the SAPO framework against the LTST, reduces the number of Brønsted acid sites and introduces more Lewis acid sites with moderate acidity. $CuAg_{2.25}$-SAPO-34 possesses a relatively higher surface Cu content than Cu-SAPO-34, although both samples have similar content of isolated Cu ions. LTST doesn't change the Cu distribution and the content of Cu ions. More importantly, surface reaction investigated by *in situ* DRIFTS reveals that the NH_3 adsorbed on the weak/moderate acid sites is more reactive for the low-temperature SCR reaction than that on the strong acid sites, independent of the acid types (Brønsted acid or Lewis acid). Based on the characterization results, it is thus concluded that the better preservation of total acid sites, higher moderate acid density and larger surface Cu amount on the $CuAg_{2.25}$-SAPO-34/H catalyst help the sample to behave better low-temperature NH_3-SCR activity than Cu-SAPO-34/H catalyst.

Author contributions

The manuscript was written through contributions of all authors. All authors have given approval to the final version of the manuscript.

Acknowledgments

We would like to thank the financial support from National Natural Science Foundation of China (Nos. 21473182, 91545104, 21606221, 21676262) and Key Research Program of Frontier Sciences, Chinese Academy of Sciences (Grant No. QYZDB-SSW-JSC040).

Appendix A. Supplementary data

Supplementary material related to this article can be found, in the online version, at doi:https://doi.org/10.1016/j.apcata.2017.12.001

References

[1] F. Liu, Y. Yu, H. He, Chem. Commun. (Camb.) 50 (2014) 8445–8463.
[2] M. Koebel, M. Elsener, M. Kleemann, Catal. Today 59 (2000) 335–345.
[3] S. Roy, M.S. Hegde, G. Madras, Appl. Energy 86 (2009) 2283–2297.
[4] J. Li, H. Chang, L. Ma, J. Hao, R.T. Yang, Catal. Today 175 (2011) 147–156.
[5] T. Zhang, J. Shi, J. Liu, D. Wang, Z. Zhao, K. Cheng, J. Li, Appl. Surf. Sci. 375 (2016) 186–195.
[6] F. Gao, J. Szanyi, Y. Wang, B. Schwenzer, M. Kollár, C.H.F. Peden, Top. Catal. 59 (2016) 882–886.
[7] L. Ma, Y. Cheng, G. Cavataio, R.W. McCabe, L. Fu, J. Li, Chem. Eng. J. 225 (2013) 323–330.
[8] D. Wang, Y. Jangjou, Y. Liu, M.K. Sharma, J. Luo, J. Li, K. Kamasamudram, W.S. Epling, Appl. Catal. B: Environ. 165 (2015) 438–445.
[9] R. Martínez-Franco, M. Moliner, P. Concepcion, J.R. Thogersen, A. Corma, J. Catal. 314 (2014) 73–82.
[10] F.D.P. Mees, L.R.M. Martens, M.J.G. Janssen, A.A. Verberckmoes, E.F. Vansant, Chem. Commun. (2003) 44–45.
[11] M. Briend, R. Vomscheid, M.J. Peltre, P.P. Man, D. Barthomeuf, J. Phys. Chem. 99 (1995) 8270–8276.
[12] D. Wang, P. Tian, M. Yang, S. Xu, D. Fan, X. Su, Y. Yang, C. Wang, Z. Liu, Microporous Mesoporous Mater. 194 (2014) 8–14.
[13] F. Gao, E.D. Walter, N.M. Washton, J. Szanyi, C.H.F. Peden, ACS Catal. 3 (2013) 2083–2093.
[14] J. Wang, D. Fan, T. Yu, J. Wang, T. Hao, X. Hu, M. Shen, W. Li, J. Catal. 322 (2015) 84–90.
[15] K. Leistner, L. Olsson, Appl. Catal. B: Environ. 165 (2015) 192–199.
[16] D. Wang, L. Zhang, J. Li, K. Kamasamudram, W.S. Epling, Catal. Today 231 (2014) 64–74.
[17] O. Mihai, C.R. Widyastuti, S. Andonova, K. Kamasamudram, J. Li, S.Y. Joshi, N.W. Currier, A. Yezerets, L. Olsson, J. Catal. 311 (2014) 170–181.
[18] X. Xiang, M. Yang, B. Gao, Y. Qiao, P. Tian, S. Xu, Z. Liu, RSC Adv. 6 (2016) 12544–12552.
[19] D. Massiot, F. Fayon, M. Capron, I. King, S. Le Calvé, B. Alonso, J.-O. Durand, B. Bujoli, Z. Gan, G. Hoatson, Magn. Reson. Chem. 40 (2002) 70–76.
[20] M. Zhang, S. Xu, J. Li, Y. Wei, Y. Gong, Y. Chu, A. Zheng, J. Wang, W. Zhang, X. Wu, F. Deng, Z. Liu, J. Catal. 335 (2016) 47–57.
[21] F. Gao, E.D. Walter, E.M. Karp, J. Luo, R.G. Tonkyn, J.H. Kwak, J. Szanyi, C.H.F. Peden, J. Catal. 300 (2013) 20–29.
[22] N. Katada, K. Nouno, J.K. Lee, J. Shin, S.B. Hong, M. Niwa, J. Phys. Chem. C 115 (2011) 22505–22513.
[23] K. Suzuki, T. Nishio, N. Katada, G. Sastre, M. Niwa, Phys. Chem. Chem. Phys. 13 (2011) 3311–3318.
[24] T. Yu, D. Fan, T. Hao, J. Wang, M. Shen, W. Li, Chem. Eng. J. 243 (2014) 159–168.
[25] J. Wang, T. Yu, X. Wang, G. Qi, J. Xue, M. Shen, W. Li, Appl. Catal. B: Environ. 127 (2012) 137–147.
[26] N. Wilken, R. Nedyalkova, K. Kamasamudram, J. Li, N.W. Currier, R. Vedaiyan, A. Yezerets, L. Olsson, Top. Catal. 56 (2013) 317–322.
[27] Y. Cao, S. Zou, L. Lan, Z. Yang, H. Xu, T. Lin, M. Gong, Y. Chen, J. Mol. Catal. A: Chem. 398 (2015) 304–311.
[28] E. Kolobova, A. Pestryakov, G. Mamontov, Y. Kotolevich, N. Bogdanchikova, M. Farias, A. Vosmerikov, L. Vosmerikova, V. Cortes Corberan, Fuel 188 (2017) 121–131.
[29] J. Xue, X. Wang, G. Qi, J. Wang, M. Shen, W. Li, J. Catal. 297 (2013) 56–64.
[30] M. Zamadics, X.H. Chen, L. Kevan, J. Phys. Chem. 96 (1992) 2652–2657.
[31] M. Zamadics, X.H. Chen, L. Kevan, J. Phys. Chem. 96 (1992) 5488–5491.
[32] H. Praliaud, S. Mikhailenko, Z. Chajar, M. Primet, Appl. Catal. B: Environ. 16 (1998) 359–374.
[33] C. Shi, L. Xu, A. Zhu, Y. Zhang, C.T. Au, Chin. J. Catal. 33 (2012) 1455–1462.
[34] A. Śrębowata, R. Baran, G. Słowik, D. Lisovytskiy, S. Dzwigaj, Appl. Catal. B: Environ. 199 (2016) 514–522.
[35] I. Lezcano-Gonzalez, U. Deka, B. Arstad, A. Van Yperen-De Deyne, K. Hemelsoet, M. Waroquier, V. Van Speybroeck, B.M. Weckhuysen, A.M. Beale, Phys. Chem.Chem. Phys.: PCCP 16 (2014) 1639–1650.
[36] M. Niwa, S. Nishikawa, N. Katada, Microporous Mesoporous Mater. 82 (2005) 105–112.
[37] C.T. Martins, B.M. Sato, O.A. El Seoud, J. Phys. Chem. B 112 (2008) 8330–8339.
[38] D. Wang, L. Zhang, K. Kamasamudram, W.S. Epling, ACS Catal. 3 (2013) 871–881.
[39] D. Wang, L. Zhang, J. Li, K. Kamasamudram, W.S. Epling, Catal. Today (2013).
[40] Q. Ye, L. Wang, R.T. Yang, Appl. Catal. A 427–428 (2012) 24–34.
[41] H.Y. Jeon, C.H. Shin, H.J. Jung, S.B. Hong, Appl. Catal. A: Gen. 305 (2006) 70–78.
[42] L. Ma, Y. Cheng, G. Cavataio, R.W. McCabe, L. Fu, J. Li, Appl. Catal. B: Environ. 156–157 (2014) 428–437.
[43] H. Sjövall, E. Fridell, R.J. Blint, L. Olsson, Top. Catal. 42–43 (2007) 113–117.
[44] G.V.A. Martins, G. Berlier, C. Bisio, S. Coluccia, H.O. Pastore, L. Marchese, J. Phys. Chem. C 112 (2008) 7193–7200.
[45] L. Wang, W. Li, G. Qi, D. Weng, J. Catal. 289 (2012) 21–29.
[46] L. Zhang, D. Wang, Y. Liu, K. Kamasamudram, J. Li, W. Epling, Appl. Catal. B: Environ. 156–157 (2014) 371–377.
[47] G.A.V. Martins, G. Berlier, S. Coluccia, H.O. Pastore, G.B. Superti, G. Gatti, L. Marchese, J. Phys. Chem. C 111 (2007) 330–339.
[48] F. Bin, C. Song, G. Lv, J. Song, S. Wu, X. Li, Appl. Catal. B: Environ. 150–151 (2014) 532–543.
[49] W. Shan, F. Liu, H. He, X. Shi, C. Zhang, Appl. Catal. B: Environ. 115–116 (2012) 100–106.